Molecular-Level Investigation of the Structure, Transformation, and Bioactivity of Single Living Fission Yeast Cells by Time- and Space-Resolved Raman Spectroscopy

Yu-San Huang,[‡] Takeshi Karashima,[§] Masayuki Yamamoto,[§] and Hiro-o Hamaguchi*[,‡]

Department of Chemistry and Department of Biophysics and Biochemistry, School of Science, The University of Tokyo, 7-3-1 Hongo, Bunkyo-ku, Tokyo 113-0033, Japan

Received January 29, 2005; Revised Manuscript Received April 23, 2005

ABSTRACT: The structure, transformation, and bioactivity of single living *Schizosaccharomyces pombe* cells at the molecular level have been studied in vivo by time- and space-resolved Raman spectroscopy. A time resolution of 100 s and a space resolution of 250 nm have been achieved with the use of a confocal Raman microspectrometer. The space-resolved Raman spectra of living *S. pombe* cells at different cell cycle stages were recorded in an effort to elucidate the molecular compositions of organelles, including nuclei, cytoplasm, mitochondria, and septa. The time- and space-resolved measurement of the central part of a dividing yeast cell showed continuous spectral evolution from that of the nucleus to those of the cytoplasm and mitochondria and finally to that of the septum, in accordance with the transformation during the cell cycle. A strong Raman band was observed at 1602 cm^{-1} only when cells were under good nutrient conditions. The effect of a respiration inhibitor, KCN, on a living yeast cell was studied by measuring the Raman spectra of its mitochondria. A sudden disappearance of the 1602 cm^{-1} band followed by the change in the shape and intensity of the phospholipid bands was observed, indicating a strong relationship between the cell activity and the intensity of this band. We therefore call this band "the Raman spectroscopic signature of life". The Raman mapping of a living yeast cell was also carried out. Not only the distributions of molecular species but also those of active mitochondria in the cell were successfully visualized in vivo.

More and more research efforts in modern physical chemistry are directed toward biology. In the past few decades, a number of sophisticated physicochemical methods have been developed and applied to biomolecules, organelles, cells, and tissues to shed new light on a variety of biological phenomena. It seems highly desirable, at this stage, to focus those efforts on a prototype living system to which different physicochemical methods can be applied from complementary standpoints. In this paper, we have chosen fission yeast *Schizosaccharomyces pombe* as a candidate for such a model living system. Fission yeast is very familiar to our life; it was isolated from East African millet beer in 1890 and was first described in 1893 (*1*). From the viewpoint of biology, it is the simplest unicellular eukaryote whose cell cycle has many features in common with those of higher eukaryotes. It is one of the most extensively used model organisms in the research fields extending from genetics to biochemistry. Nevertheless, *S. pombe* has rarely been selected to be the sample of physicochemical investigations (*2*−*5*). Considering its significance in biology, we believe that the physicochemical studies of living *S. pombe* cells will provide a firm basis for the understanding of life at the molecular level.

* To whom correspondence should be addressed: Department of Chemistry, School of Science, The University of Tokyo, 7-3-1 Hongo, Bunkyo-ku, Tokyo 113-0033, Japan. E-mail: hhama@chem.s.u-tokyo.ac.jp. Telephone: +81-3-5841-4327. Fax: +81-3-3818-4621.

[‡] Department of Chemistry.

[§] Department of Biophysics and Biochemistry.

It is needless to say that the deeper we want to look into the nature of life, the more molecular information we need to collect from living cells. Unlike in fixed (dead) cells, however, the molecular compositions and distributions in living cells change continuously from time to time and place to place throughout the course of the cell cycle. This fact makes the molecular-level study of living cells highly difficult. In recent years, a number of cell cycle events have been studied with the use of biological and biochemical approaches. However, these methods are intrinsically lacking in time and space specificity; molecular information obtained by those methods is always time- and space-averaged. How can we know what molecules really exist in a living cell? How can we measure the structural changes of those molecules in vivo? In our study, we use time- and space-resolved Raman spectroscopy. Raman spectroscopy provides a time resolution of picoseconds or shorter (100 s in the present experiments) and a space resolution of a few hundred nanometers. In this respect, it surpasses any existing biological and biochemical methods. The high information content at the molecular level is also unique to Raman spectroscopy. For these reasons, it is now used extensively for investigating a wide range of biological samples. If we confine our attention to living cells, prokaryotic cells (*6*, *7*) as well as eukaryotic cells (*3*−*5*, *8*−*11*), including human cells (*12*−*18*), have already been studied, and more and more will be investigated soon. Although most of the cell samples in those papers were reported to be "living cells", it is not clear

10.1021/bi050179w CCC: $30.25
Published on Web 07/09/2005

whether the cells were really living. In a previous paper on a single living *S. pombe* cell (*3*), we reported the discovery of a still unidentified Raman band located at 1602 cm^{-1}. In the following publication (*5*), we found a strong relationship of this band with the mitochondrial metabolic activity and called it "the Raman spectroscopic signature of life". In the following, we discuss the Raman spectra of single living *S. pombe* cells that were obtained under carefully prepared physiological conditions in which we checked that the cells were actually dividing. We start with the space-resolved Raman spectra of single living yeast cells in different phases of the cell cycle, namely, the G2, M, and G1/S phases. Raman spectra obtained from several points of the same single living cell in the three phases are compared to show a marked variation of the molecular compositions in various organelles within the cell. We discuss those spectra with reference to the well-established biological and physicochemical knowledge. Then, we describe the time- and space-resolved Raman spectra of a dividing yeast cell. We show that we can not only measure separately the organelles in a living cell but also trace the molecular-level change of a cell throughout its cell cycle. The time- and space-resolved Raman spectra of a yeast cell treated with a respiration inhibitor (KCN) are discussed next. The addition of the respiration inhibitor immediately caused dramatic changes in the spectra of the mitochondria, showing the lowering of the mitochondrial metabolic activity and the subsequent degradation of the membrane structure. These changes correspond to the early dying processes of the *S. pombe* cell, which are clearly monitored by the Raman spectroscopic signature of life. The Raman mapping of a living yeast cell is discussed in the last section. The molecular distribution in the cell is visualized by characteristic Raman bands of proteins, phospholipids, and polysaccharides as well as the 1602 cm^{-1} band and is compared with the GFP image obtained just before the Raman measurements. The mapping patterns also show that the molecular distributions in a cell tend to be symmetric with respect to the center irrespective of the cell cycle stage. The power of Raman mapping, which does not require any dyeing or genetic manipulation of the cell, is thus demonstrated.

EXPERIMENTAL PROCEDURES

Samples. To visualize the nuclei of *S. pombe* cells, a green fluorescent protein (GFP)[1] fused with SV40 NLS (nuclear localization signal) and glutathione *S*-transferase (GST) was expressed from the *adh* promoter that was integrated together with a kanamycin resistance gene at the *leu1* locus of a wild-type strain. Similarly, a GFP fused with the signal sequence from *Saccharomyces cerevisiae* Cox4 (cytochrome oxidase subunit IV) was used as a mitochondrial marker (*19*). These cells were cultured in YE liquid medium supplemented with 100 mg/L Geneticin (Sigma) before the experiments. For the preparation of samples for Raman spectroscopic measurements, the growing cells and the YE broth or water were placed between a slide glass and a cover glass. The edge of the cover glass was sealed with Vaseline to prevent the volatilization of water. We did not use any coating on the slide glass to immobilize the cells. Instead, we fixed them by putting a small quantity of the sample between the slide and cover glasses and making the thickness of the sample layer close to the diameter of the yeast cell. For the observation of the effect of the respiration inhibitor on a living yeast cell, we dispersed living cells in water and immobilized the cell on a ConA-coated glass-bottom dish. Respiration inhibitor was added to the sample by a pipet to start the time-resolved measurements. KCN was chosen as the respiration inhibitor in this study. The final concentration of KCN was ~0.25 mM. All the chemicals, including L-α-phosphatidylcholine (from fresh egg yolk, Sigma), were commercially obtained and were used as received.

Apparatus and Methods. We used a confocal Raman microspectrometer (Nanofinder, Tokyo Instrument Inc.). The 632.8 nm line (3 mW on the sample stage) of a He−Ne laser (Melles Griot 05-LHP-991) was focused on a position in a selected yeast cell with the help of a fluorescence microscope (Olympus IX50). A 100× oil immersion objective (Olympus UPlanFI100) with an NA of 1.3 was used. The backward Raman scattering was collected by the same objective. After passing through a 100 μm pinhole, the scattered light was introduced into the spectrometer and detected by a thermoelectrically cooled (−70 °C) CCD detector (Andor DU420-BV). Spatial resolutions of 250 nm in the lateral direction and 1.7 μm in the depth direction were achieved. The lateral space resolution of 250 nm was confirmed by measuring the intensity rise at the edge of lines on a Ronchi Ruling glass slide (Edmund Optics, 600 lp/mm, Soda Lime type). The observed laser beam size was ~1 μm. A digital camera (Olympus DP70) mounted on the same microscope was used to obtain the fluorescence microscope images. Because GFP is excited by only blue light, the He−Ne laser line does not excite fluorescence from GFP during the Raman spectroscopic measurements. All measurements were carried out at room temperature. All the spectra and images were background subtracted.

Different exposure times were used according to the purposes of the measurements. The exposure time for the space-resolved Raman measurements was as long as 300 s, so we can obtain a higher signal-to-noise ratio to collect as much information about the molecular composition of a cell as possible. On the other hand, for the measurement of time-resolved spectra of a respiration inhibitor-treated yeast cell, the exposure time was reduced to 100 s to trace the quickly changing molecular compositions in the cell. In the Raman mapping measurement, the excitation laser spot scanned across a yeast cell. The cell was translated by a piezoelectric stage horizontally with a 0.5 μm step in both *x* and *y* directions. Images of the cell were generated using the 1 or 2 s integrated intensity of the Raman bands collected from each position of the laser spot. It took ~20 min to complete the entire scanning of the cell. Images of different Raman bands were obtained simultaneously.

RESULTS AND DISCUSSION

Space-Resolved Raman Spectra of Living Yeast Cells at Different Cell Cycle Stages

Figure 1 schematically shows the cell cycle of *S. pombe*. In the G2 (gap-2) phase, the cell grows to prepare for division with duplicated chromosomes in the nucleus. In the M

[1] Abbreviations: GFP, green fluorescent protein; He−Ne laser, helium−neon light amplified by stimulated emission of radiation; CCD, charge-coupled device; cm^{-1}, wavenumber.

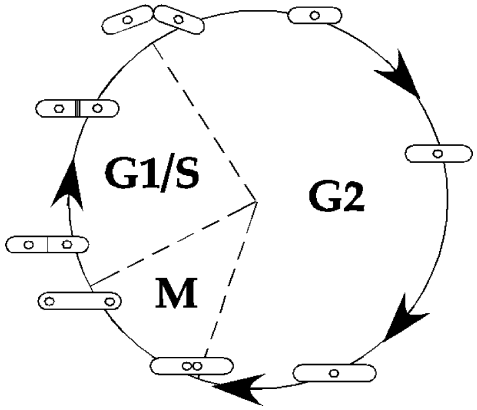

FIGURE 1: Cell cycle of *S. pombe*. *S. pombe* has a very short G1 phase; therefore, we use the notation G1/S.

(mitosis) phase, the duplicated chromosomes are segregated and the nucleus is split into two portions. The split nuclei then move toward the two ends of the cell. A septum is formed in the G1 (gap-1) phase to separate the cell into two moieties. In the S (synthesis) phase, the division is completed and two daughter cells are formed. The chromosome duplication takes place in this phase, preparing for the next division. It is known that *S. pombe* has a very short G1 phase under normal vegetative conditions. This fact makes the G1 phase of *S. pombe* unclear. In the following, we use the notation G1/S.

The space-resolved Raman spectra of single living *S. pombe* cells in the G2 (panel a), M (panel b), and G1/S (panel c) phases are shown in Figure 2. The GFP images obtained just before the Raman measurements are also shown at the top of this figure. The positions from where Raman spectra are measured are denoted by letters A−E for the G2 and M phases and A−G for the G1/S phase. The cell cycle stages are known from the length of a cell, the number of nuclei, and the appearance of a septum. Note that, in these experiments, measured cells were dispersed in water for 1 h without any nourishment so that the cell cycle was slowed to allow a long exposure time of 300 s. All the observed Raman spectra sharply reflect the molecular compositions at the positions from where they are measured.

The Raman spectra shown in Figure 2 are grossly categorized into four types: those from nuclei (A-e, B-c, B-d, C-c, and C-d), those from mitochondria (A-a−A-d, B-a, B-e, B-f, and C-e), that from septum (C-g), and those from cytoplasm (B-b, B-g, C-a, C-b, and C-f). It is not obvious from Figure 2 alone that spectra A-a−A-d, B-a, B-e, B-f, and C-e can be ascribed to mitochondria. However, in a separate experiment with a cell whose mitochondria are labeled with GFP, it is confirmed that they are in fact measured from mitochondria (*5*). The spectra from nuclei and those from cytoplasm are similar with one another, though a small difference is notable. They are all dominated by known protein Raman bands. The spectra obtained from mitochondria resemble those of phospholipids, and that of the septum is dominated by carbohydrate bands as discussed in detail in the following sections.

In the G2 phase spectra (Figure 2A), spectra A-a and A-b resemble each other as do spectra A-c and A-d. This finding indicates that the molecular composition in a yeast cell in the G2 phase is symmetric with respect to the center. It seems

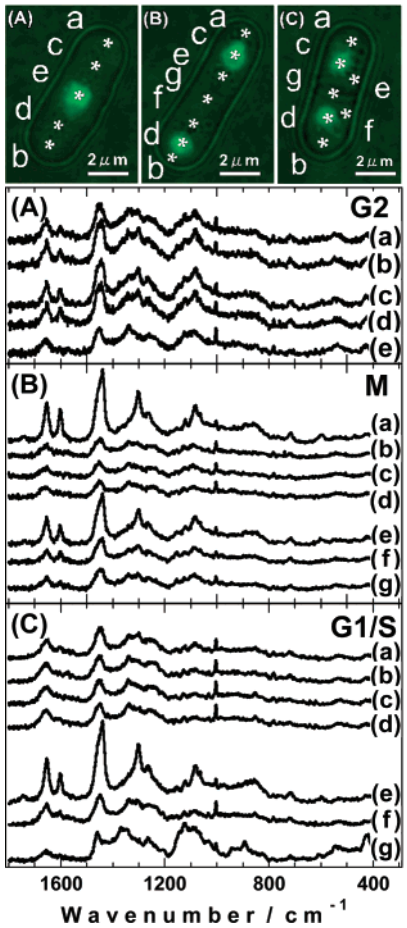

FIGURE 2: Space-resolved Raman spectra of living yeast cells in different cell cycle phases. GFP images obtained under the same microscope just before the Raman spectroscopic measurements are also displayed. The letters denote the positions in the cell from which the Raman spectra were recorded.

that a *S. pombe* cell is prepared for the future division well beforehand so that the synthesized molecules and organelles are evenly distributed to the two moieties of the cell when the division starts. We will come back to this point later with more detailed molecular distribution data in the whole cell based on the Raman mapping method.

Raman Spectra of GFP-Labeled and Unlabeled Organelles. As described in Experimental Procedures, the 632.8 nm line of a He−Ne laser does not excite fluorescence from GFP during the Raman spectroscopic measurements. However, Raman scattering from GFP may affect the observed Raman spectra through the preresonance effect. So, we measured and compared the Raman spectra of GFP-labeled and unlabeled nuclei and mitochondria. The space-resolved Raman spectra of a nucleus-labeled cell (cell 1) and a mitochondria-labeled cell (cell 2) are shown in Figure 3. The Raman spectra of nuclei with and without GFP labeling are compared in spectra a and b of Figure 3. They are much the same, and no appreciable difference that can be ascribed to GFP is found. Spectra c and d of Figure 3 show the Raman spectra of mitochondria with and without GFP labeling. Again, these two spectra resemble each other, except for the intensity of a band at 1602 cm^{-1}. As shown later, the intensity variation of this 1602 cm^{-1} band has nothing to do with GFP labeling. It is thus confirmed that GFP labeling does not affect appreciably the Raman spectra of nuclei and mito-

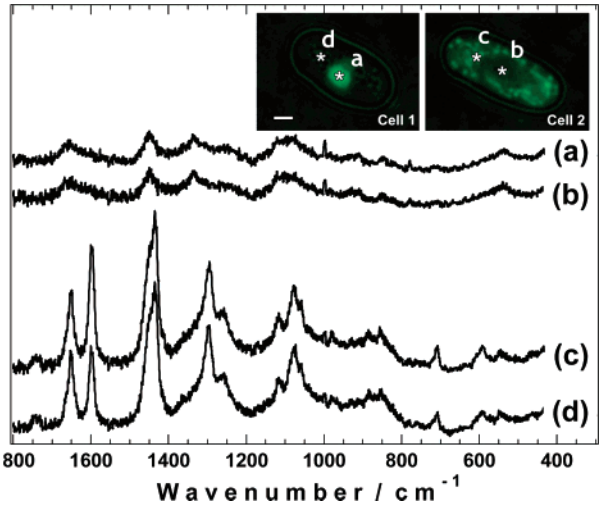

FIGURE 3: Space-resolved Raman spectra measured from a cell with its nucleus labeled with GFP (cell 1) and a cell with its mitochondria labeled with GFP (cell 2). The short bar in the photograph measures 1 μm.

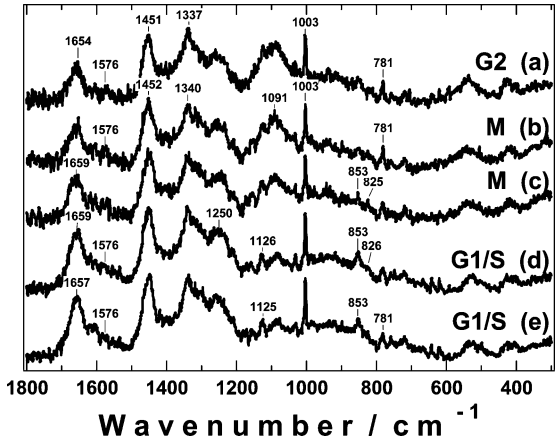

FIGURE 4: Raman spectra of nuclei in the G2 (a), M (b and c), and G1/S (d and e) phases.

chondria, which will be discussed in detail in the following sections.

Raman Spectra of Nuclei in Different Cell Cycle Phases. The Raman spectra of nuclei in the G2 (4-a), M (4-b and 4-c), and G1/S (4-d and 4-e) phases are compared in Figure 4. They are identical with those already displayed in Figure 2. These five spectra look similar with one another and are all dominated by the known Raman bands of proteins. In addition, weak bands that can be assigned to nucleic acids (*20*) are found at 781 and 1576 cm^{-1}. According to the result of a biological component analysis of isolated nuclei, the proportional DNA/RNA/protein chemical composition in a *S. pombe* nucleus is 1/9.4/115 (*21*). This ratio means that proteins are ~10 times more abundant in the isolated nucleus than nucleic acids. The in vivo Raman spectra observed in this study indicate that a similar ratio also applies to living nuclei.

The prominent protein bands observed in Figure 4 are identified as the amide I mode of the main chain (1655−1660 cm^{-1}), the CH bending of the aliphatic chain (1450 and 1340 cm^{-1}), the amide III mode of the main chain (1250−1300 cm^{-1}), and the breathing mode of the phenylalanine residue in the subchain (1003 cm^{-1}). It is well established that the frequencies of the amide I and III bands are sensitive markers of the secondary structure of the protein main chain (*22*). They can be used for the determination of the secondary structure content of proteins in biological samples (*23*). In our experiments, the amide I band is observed in the range of 1654−1659 cm^{-1} for all the phases, G2, M, and G1/S. Although this center frequency can be assigned to the α-helix structure (~1655 cm^{-1}) (*24*), we need to carefully examine the contour of this broad band as well. A band fitting analysis of a spectrum with a better signal-to-noise ratio is necessary for further quantitative discussion of the existence of the β-sheet, random coil (~1665−1670 cm^{-1}) (*24*), and other unfolded structures that appear at higher wavenumbers. New insight into the secondary structure of proteins in a living cell, which can now be obtained by Raman spectroscopy, is of great interest in connection with the presence of natively unfolded proteins (*24*−*26*), which has been discussed intensively in the past few years.

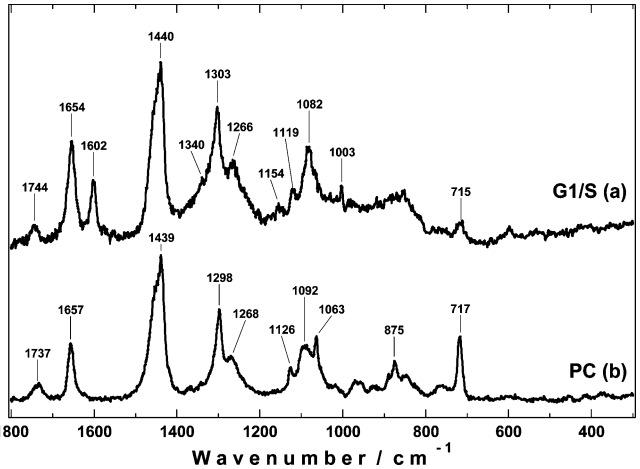

FIGURE 5: Comparison of the Raman spectra of mitochondria (a, selected from Figure 2) and phosphatidylcholine (b).

The broad band centered at 1100 cm^{-1} and the doublet at 853 and 825 cm^{-1} in the G1/S phase spectra (spectra d and e of Figure 4) are also noteworthy. It is known that the bands in the 1100 cm^{-1} region sensitively reflect the structural change of the hydrocarbon chain and the lipid−protein interaction (*23*, *27*). The bands at 853 and 825 cm^{-1} are assigned to the Fermi doublet of a ring-breathing vibration and the overtone of an out-of-plane ring-bending vibration of tyrosyl residues. The I_{853}/I_{825} intensity ratio is known to be an indicator of the H bonding strength of the phenolic hydroxyl group (*28*). If reliable biochemical data are available for the compositions of proteins existing in a living *S. pombe* nucleus, we will be able to discuss in more detail those Raman spectroscopic features from the viewpoint of protein structures and their changes following the cell cycle.

Raman Spectrum from Mitochondria. In Figure 5, the Raman spectrum from mitochondria in the G1/S (spectrum a) stage is compared with that of phosphatidylcholine (spectrum b). The spectra of mitochondria in other cell cycle stages resemble that in spectrum b of Figure 5, except for the intensity of the 1602 cm^{-1} band relative to that of the 1654 cm^{-1} band. Apart from this 1602 cm^{-1} band, all prominent bands in spectrum b of Figure 5 are assigned to the known phospholipid vibrations with reference to the assignments of the spectrum of phosphatidylcholine (*29*, *30*).

The 1744 cm^{-1} band is undoubtedly assigned to the C═O stretch of the ester linkage (*30*). The band at 1654 cm^{-1} is due to the C═C stretch of the cis −CH═CH− linkage of the unsaturated lipid chains. The strong 1440 cm^{-1} band is ascribed to the CH bending modes, including CH_2 scissors and CH_3 degenerate deformation of the hydrocarbon chains. The 1303 cm^{-1} band is assigned to the in-phase CH_2 twisting mode. The band at 1266 cm^{-1} is assigned to the C═C−H in-plane bend of the cis −CH═CH− linkage. The skeletal C−C stretch modes in the 1000−1150 cm^{-1} region are known to be sensitive to the conformation of the hydrocarbon chains (*27*). The bands at 1062 and 1122 cm^{-1} are assigned to the out-of-phase and in-phase modes of the all-trans chain (*31*−*33*), while the band at 1082 cm^{-1} is attributed to the gauche conformation. The ratio of the intensity of the gauche band to the trans is larger in spectrum a of Figure 5 than in spectrum b, suggesting that the hydrocarbon chains of the mitochondrial membrane are conformationally less ordered than that in pure phosphatidylcholine. Since the Raman features in the 1000−1150 cm^{-1} region resemble those of an L-α-dipalmitoyl phosphatidylcholine solution (*29*) and those of DOPC (1,2-dipalmitoyl-*sn*-glycero-3-phosphocholine) in the liquid crystal phase (*34*), we come to a conclusion that the phospholipid bilayer of the mitochondria in a yeast living cell is in a disordered state analogous to that in the liquid crystal state and/or in the liquid state. A Raman band due to the phospholipid headgroup is observed around 715 cm^{-1} (717 cm^{-1} for phosphatidylcholine) (*29*, *30*), though its relative intensity is much lower than that of pure phosphatidylcholine. In addition, several protein bands are observed in spectrum a in Figure 5. The amide I mode may be responsible for the broad and weak feature that underlies the 1654 cm^{-1} band. The CH bending modes of proteins may also overlap with the 1440 cm^{-1} band. The bands at 1340 cm^{-1} (CH_2 deformation) and 1266 cm^{-1} (amide III), the broad band at 1154 cm^{-1} (C−C and C−N stretching), and the sharp band at 1003 cm^{-1} (phenylalanine residues) are ascribed to proteins.

As described above, the predominance of lipid Raman bands is observed for all the mitochondria examined in the cells in various cell cycle phases. This finding is in sharp contrast to the protein-dominant Raman spectra of cytoplasm and nuclei. The most interesting finding with the Raman spectra of mitochondria, however, is the prominent band observed at 1602 cm^{-1} and its intensity variation relative to the other phospholipid bands. This finding will be discussed in more detail in the following sections.

Finally, we note the difficulty in measuring the space-resolved Raman spectra of mitochondria from a living cell. Mitochondria are smaller in size and move faster than the nucleus and septum. As a result, a measurement may collect Raman scattering from both mitochondria and the cytoplasm surrounding them simultaneously. For instance, the spectra in Figure 2 (A-a−A-d) contain both the characteristic bands of mitochondria and those of proteins in cytoplasm. The intensities of the bands of proteins at 1654 (amide I), 1340 (CH_2 deformation), 1250 (amide III), and 1003 cm^{-1} (phenylalanine ring breathing mode) are observed more strongly than the other mitochondria spectra. To avoid this ambiguity, the Raman mapping method is used in the following section to discuss the distribution of mitochondria in a *S. pombe* cell. The Raman mapping result shows good correspondence with the GFP fluorescence image of the mitochondria of the same cell. It also confirms that the 1602 cm^{-1} band is observed solely from mitochondria.

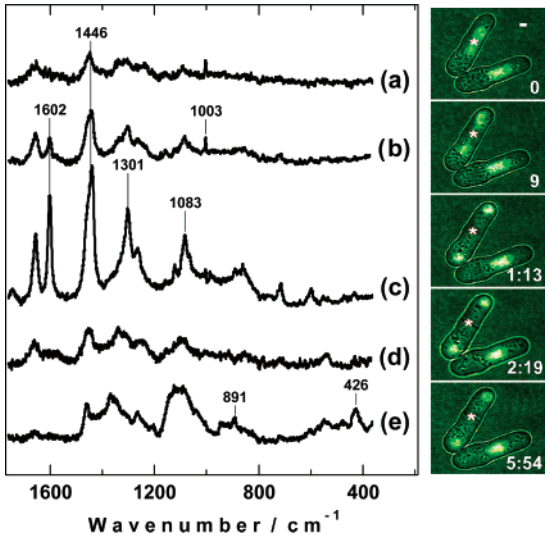

FIGURE 6: Time- and space-resolved Raman spectra of the central part of a dividing *S. pombe* cell. The laser beam spot is denoted with an asterisk. The short bar in the photograph measures 1 μm.

Time- and Space-Resolved Raman Spectra of a Dividing Yeast Cell

In the preceding section, we compared and discussed the space-resolved Raman spectra obtained from the three different cell cycle stages of different *S. pombe* cells. If we use the time- and space-resolved Raman method, we are able to compare the Raman spectra obtained from the same *S. pombe* cell in different cell cycle phases. However, because of the limitation due to the required long exposure time (100−300 s), we were able to perform only the experiment in which the excitation laser beam was fixed at a particular point of a cell without scanning. The resultant time- and space-resolved Raman spectra are shown in Figure 6. The GFP images indicating the positions and numbers of the nuclei are also shown together. In this experiment, we focused the laser beam at the center of a selected *S. pombe* cell and measured the Raman spectra during the cell cycle. We have already reported a similar experiment with a 100 s exposure time in a previous paper (*5*). In the present experiment, we use a longer exposure time (300 s) to achieve a higher signal-to-noise ratio so that we can discuss the details of the time- and space-resolved Raman spectra. We noticed during this experiment that it took a longer time for the selected *S. pombe* cell to complete the cell cycle than it did for the other nearby cells. It is possible that the heating by the laser beam slows the cell cycle to some extent.

With the help of the GFP images, we are able to determine the cell cycle stages for each of the Raman spectra shown in Figure 6. The Raman measurement starts from the early M phase (spectrum a of Figure 6, 0 min), in which a dividing nucleus is located at the center of the cell. At 9 min (spectrum b of Figure 6), the divided nuclei are put apart symmetrically toward the perimeter of the cell. At the G1/S phase (spectrum c of Figure 6; 1 h, 13 min), the nuclei are completely separated and located at the two ends of the cell. In the following G1/S period, a septum starts to form from the

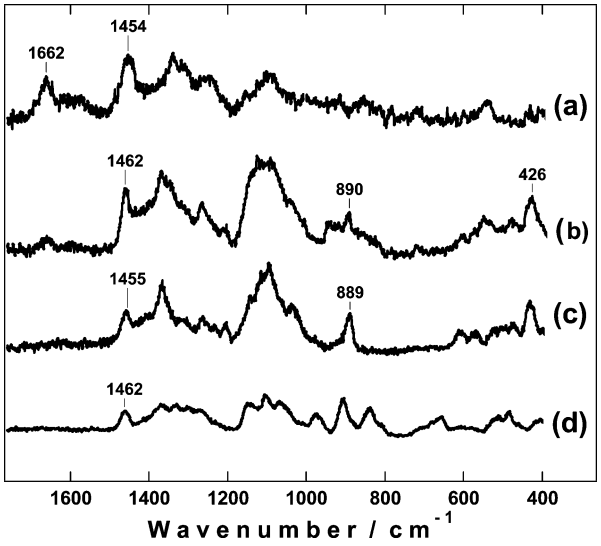

FIGURE 7: Comparison of the Raman spectra of the primary septum (a), matured septum (b), β-1,3-glucan (c), and mannan (d).

plasma membrane (spectrum d of Figure 6, 2 h, 19 min), and it eventually becomes mature (spectrum e of Figure 6, 5 h, 54 min).

As the cell division proceeds, the Raman spectrum changes drastically, reflecting the changes in molecular composition of the organelles existing at the central part of the cell. The Raman bands observed at 0 min (spectrum a of Figure 6) are ascribed to the proteins in the nucleus. The spectrum at 9 min (spectrum b) is a hybrid of those of the mitochondrion and cytoplasm, indicating that mitochondria start to be generated at the central part of the cell. At 1 h, 13 min (spectrum c), the Raman spectrum is dominated by the phospholipid bands of mitochondria. We conclude that mitochondria do exist at the center of the cell at this stage. In addition, the unidentified 1602 cm^{-1} band is observed strongly. The intensity of this band is significantly higher than those observed in the space-resolved experiment in Figure 2. This result is of interest with regard to the relevance of the 1602 cm^{-1} band to the metabolic activity of a mitochondrion. Since the cells used for the time- and space-resolved measurement were dispersed in YE broth, a better nutrient condition was provided than in the space-resolved measurements. The stronger 1602 cm^{-1} band in spectrum c is indicative of higher metabolic activities in a *S. pombe* cell in YE broth.

Spectra d (2 h, 19 min) and e (5 h, 54 min) of Figure 6 are obtained from the septum. In Figure 7, these spectra are compared with those of β-1,3-glucan (Figure 7c) and mannan (Figure 7d), which are considered the two main components of a septum (*35*). Observed spectra a (6d) and b (6e) of Figure 7 are distinct from each other, reflecting the evolution of the septum on going from 2 h, 19 min (6d) to 5 h, 54 min (6e). Spectrum 7b looks very like with that of β-1,3-glucan, indicating that glucan is the principal molecular component of the matured septum. On the other hand, the spectrum of mannan has little similarity with either spectrum 7a or 7b.

Although Raman spectroscopic studies of polysaccharides are scant, the normal-mode analysis of disaccharides has been reported (*36*, *37*). With reference to the potential energy distributions obtained by this analysis, the band at 1454 cm^{-1} in the primary septum (Figure 7a) is assigned to the CH bending vibration of the CH_2OH group of reducing pyranose rings. The corresponding band at 1462 cm^{-1} in the matured septum (Figure 7b) is assigned to the same vibration of nonreducing pyranose rings. The 890 cm^{-1} band, which is not observed in Figure 7a, but is observed in Figure 7b, is assigned to the CO stretch of the glycosidic linkage. Thus, the change in the CH bend frequency and the appearance of the Raman band at 890 cm^{-1} upon going from spectrum 7a to spectrum 7b correspond very well to the maturing process of the septum, showing the gradual polymerization of the saccharide rings. The bands observed in the 1050−1150 cm^{-1} region can be assigned to the C−C and C−O stretch modes of the pyranose rings. The 426 cm^{-1} band is ascribed to the C−C−C and C−C−O bending modes. Besides the Raman bands of polysaccharides discussed above, the amide I bands are observed at 1662 cm^{-1} for both the primary and matured septa.

In this way, the changes in the molecular compositions in the central part of the yeast cell have been successfully traced by time- and space-resolved Raman spectroscopy. It clearly shows the changes that occur along with the organelle existing at the central part changing from a dividing nucleus to mitochondria and then to a septum. It even clarifies the molecular-level maturing process of a septum.

The 1602 cm^{-1} Band: The Raman Spectroscopic Signature of Life

Knowing that the Raman band at 1602 cm^{-1} arises from a still unidentified molecular species existing in mitochondria (*5*), we have carried out the following two experiments to obtain more information about its origin. First, we measured the Raman spectra of biological molecules that are known to exist in a mitochondrion, including flavin adenine dinucleotide (FAD), nicotinamide adenine dinucleotide (NAD), adenosine diphosphate (ADP), adenosine triphosphate (ATP), cytochrome *a*, and cytochrome *c* (spectral data not shown). However, none of these spectra showed a peak at 1602 cm^{-1}. We also searched for a biological molecule that shows a strong and isolated peak at 1602 cm^{-1} in the literature, but only in vain. It seems that the Raman band at 1602 cm^{-1} originates from a molecular species existing only in a living yeast cell and that this molecular species cannot be extracted from the cell by biochemical methods.

Next, we carried out an experiment in which the metabolic activity of the cell was deliberately lowered by adding a cellular respiration inhibitor. In the course of the space-resolved Raman experiments described in the preceding section, we noticed that the intensity of the 1602 cm^{-1} band exhibited a dependence on the nutrient conditions of the yeast cell; it was strong in YE broth but weak in pure water. Considering the fact that the 1602 cm^{-1} band is observed solely from mitochondria, we suspect that it reflects the strength of the mitochondrial metabolic activity in a living yeast cell. It would therefore be of considerable interest to look into the effect of a respiration inhibitor on the intensity of the 1602 cm^{-1} band. We used KCN as the cellular respiration inhibitor in the following experiment. It is known to form a stable coordination complex with cytochrome *c* oxidase in mitochondria, blocking the cellular respiration effectively (*38*). The time- and space-resolved Raman spectra

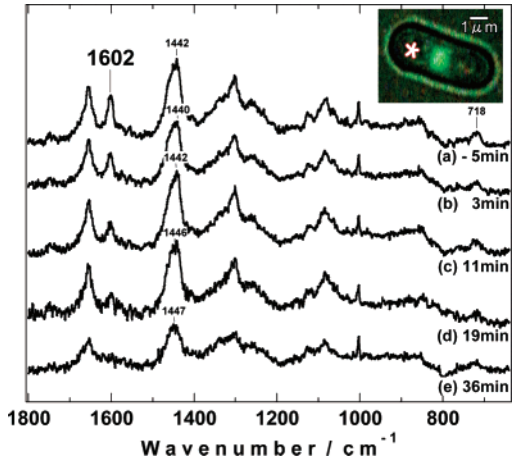

FIGURE 8: Time- and space-resolved Raman spectra of a respiration inhibitor-treated yeast cell. The position of the laser beam on the cell is denoted with an asterisk.

of a KCN-treated yeast cell are shown in Figure 8. In this experiment, we fixed the laser spot (shown with an asterisk) to mitochondria in a cell and observed the spectral changes induced by the addition of KCN. Five minutes before KCN was added, the spectrum contains a strong band at 1602 cm^{-1} in addition to the phospholipid bands at 1655, 1446, and 1300 cm^{-1} (Figure 8a). Three minutes after the addition of KCN (Figure 8b), the intensity of the 1602 cm^{-1} band decreases appreciably, while the other phospholipid bands remain unchanged. The 1602 cm^{-1} band becomes weaker as time goes on (spectra 8c and 8d), and it eventually disappears at 36 min (spectrum 8e). Concomitantly, the phospholipid signatures gradually change from well-shaped peaks to diffuse broad bands. The protein band at 1003 cm^{-1} does not change, and no additional peaks appear throughout the time course of the experiment.

The 1602 cm^{-1} band shows a surprisingly fast response to the respiration inhibitor KCN. In this experiment, the added cyanide anion CN^- must diffuse first through the solvent water to the cell and then through the cell wall, the cytoplasm, and the outer membrane of a mitochondrion before it reaches the inner membrane, where it acts as a respiration inhibitor. If the time needed for these diffusion processes is taken into account, the observed response time of a few minutes means an almost "instantaneous" action of CN^- on the species represented by the 1602 cm^{-1} band. The molecular species responsible for this band is most probably involved in the respiration chain, downstream of the acting site of CN^-, or in a mitochondrial metabolic process that is directly connected to it.

To obtain more detailed spectral information about the species giving rise to the 1602 cm^{-1} band, we produced a difference spectrum between spectra a and b of Figure 8 and spectra a and c of Figure 8. Just after the addition of KCN, the effect must be restricted to the neighborhood of the acting site of CN^-, i.e., to those molecules involved in the respiration chain and/or in a metabolic process in the mitochondria. In fact, the spectra 3 and 11 min after the addition of KCN (spectra b and c of Figure 8, respectively) look much the same as that before the KCN treatment (Figure 8a), except for the intensity of the 1602 cm^{-1} band. Thus, if we subtract the spectrum 8b or 8c from spectrum 8a, we obtain a spectrum that is ascribed primarily to the species

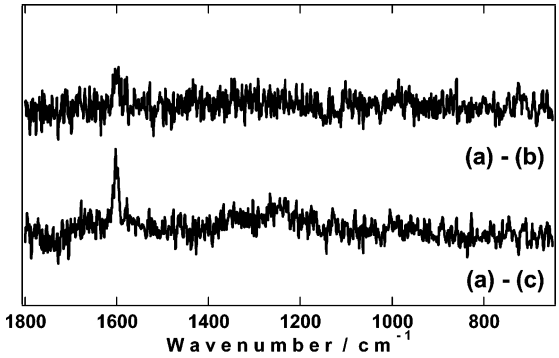

FIGURE 9: Difference spectra (spectrum 8a − spectrum 8b and spectrum 8a − spectrum 8c).

responsible for the 1602 cm^{-1} band. The resultant difference spectra are displayed in Figure 9. They show only one strong band at 1602 cm^{-1} and no other distinct peaks except for a broad feature in the 1100−1400 cm^{-1} region. From this characteristic spectral pattern in the difference spectrum, we can make the following points. In the first place, the possibility of assigning the 1602 cm^{-1} band to a ring stretch mode of an aromatic amino acid residue (*4*, *15*) is ruled out. If this band arose from a phenyl ring, it must have been accompanied by other bands, including a strong band at 1003 cm^{-1}. The pattern might be an indication of a diatomic species having only one normal mode or a small molecular species having only one Raman active normal mode in the measured wavenumber region. Alternatively, it might be a consequence of the resonance Raman effect in which only one normal mode is selectively enhanced to predominate the spectrum.

It is quite unlikely that the small molecule possibly responsible for the 1602 cm^{-1} band exists in a mitochondrion as abundantly as phospholipids do. Note that a mitochondrion has a double-membrane structure that is extremely rich in phospholipids. Rather, the high intensity of the 1602 cm^{-1} band is more reasonably explained in terms of the resonance Raman effect. It is well-known that Raman intensities are significantly enhanced if the exciting laser line comes into resonance with an electronic absorption band (*39*). The enhancement factor can be as large as 10^4, if the resonant electronic transition is fully allowed. Therefore, a resonant molecular species existing in a mitochondrion can give rise to a Raman band as strong as those of phospholipids, even if its concentration is very low. We suspect that the 1602 cm^{-1} band originates from a molecule that has a strong electronic absorption around the excitation wavelength (632.8 nm). Several biological molecules, including carotenoids, chlorophiles, and heme proteins, are known to have allowed electronic transitions in the 600 nm region. The chromophores of these molecules consist of conjugated C═CH−C and/or C═N−C systems, and consequently, the reported resonance Raman spectra of those pigments always contain C−C and/or C−N single-bond stretch bands, in addition to the C═C and/or C═N double-bond stretch bands that might well give the 1602 cm^{-1} band. Thus, the spectral patterns in Figure 9 are not consistent with the known resonance Raman spectra of those pigments. The molecular species responsible for the 1602 cm^{-1} band seems to be an unknown molecular species, most probably a small molecule with only one highly resonance-enhanced Raman band, existing as an intermediate in the cellular respiration chain or in the metabolic cycle in

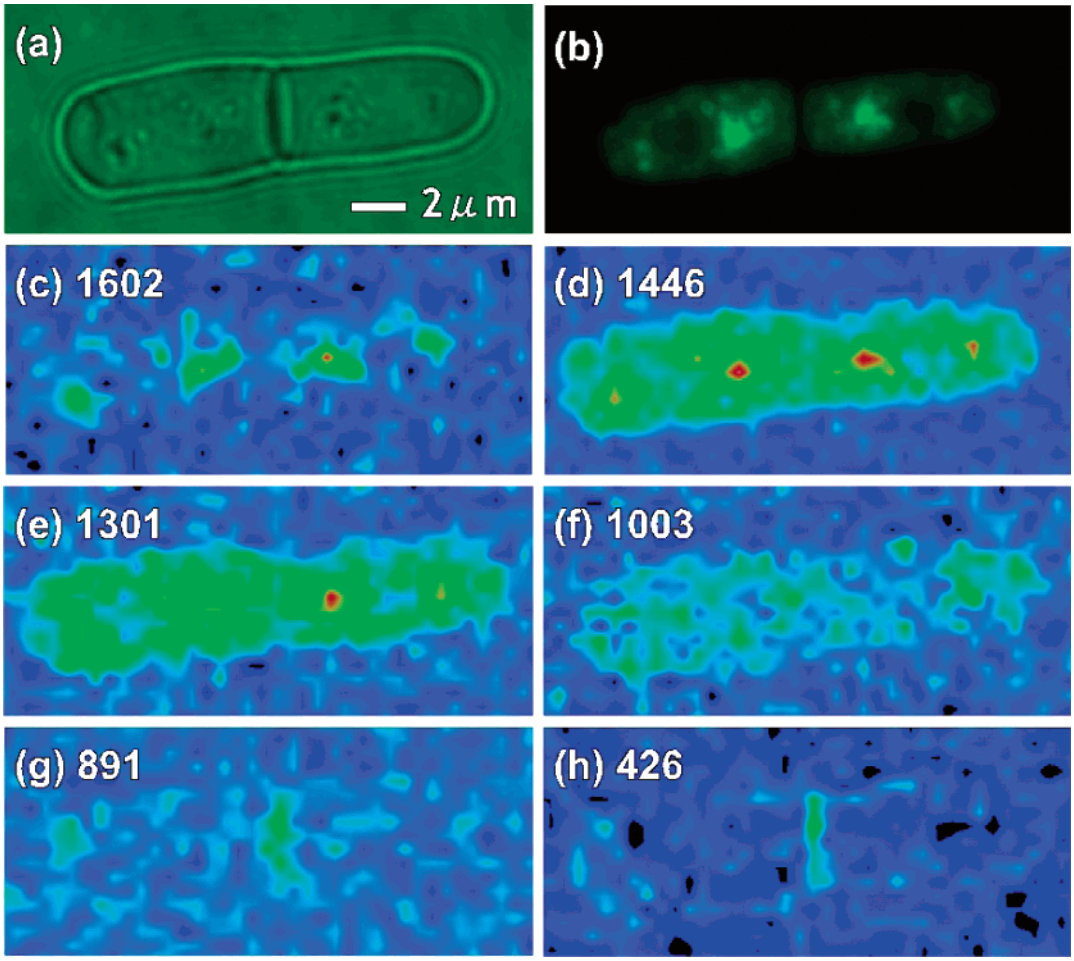

FIGURE 10: Raman mapping of a living G1/S phase *S. pombe* cell: (a) microscopic optical image, (b) GFP image, (c) 1602 cm^{-1}, (d) 1446 cm^{-1}, (e) 1301 cm^{-1}, (f) 1003 cm^{-1}, (g) 891 cm^{-1}, and (h) 426 cm^{-1}.

a mitochondrion. We certainly need more experiments to finally identify the origin of the 1602 cm^{-1} band.

In addition to the sudden decrease in the intensity of the 1602 cm^{-1} band, we also observe gradual changes in the phospholipid bands. Compared with the protein Raman band at 1003 cm^{-1}, the intensity of the phospholipid bands in Figure 8 decreases in a parallel fashion and the peak position of the CH bend band changes from 1442 cm^{-1} in Figure 8a to 1447 cm^{-1} in Figure 8e, together with the decrease in the intensity of the phospholipid headgroup band at 718 cm^{-1}. These spectral changes can be attributed to the degradation and disappearance of the double-membrane structure of mitochondria. The eventual spectrum at 36 min (Figure 8e) looks more like that of cytoplasm (see spectrum C-a of Figure 2) than that of phosphatidylcholine, indicating clearly the lowered concentration of phospholipids and, most probably, the dissociation of the mitochondria into cytoplasm.

We have found that the addition of KCN affects a mitochondrion of a living yeast cell in two steps. First, the cellular respiration is inhibited by the action of CN^- on cytochrome *c* oxidase, and the metabolic activity of the mitochondrion is lowered. This process has been monitored by the decrease in the intensity of the band at 1602 cm^{-1}. Second, because of the lowered metabolic activities, the double-membrane structure of the mitochondrion deteriorates and eventually is destroyed, as probed by the changes in the Raman bands of phospholipids. The still unidentified band at 1602 cm^{-1}, the Raman spectroscopic signature of life, has thus shed the first light upon the *primary dying process* of the KCN-treated *S. pombe* cell.

Raman Mapping of Single Living S. pombe Cells

The space-resolved Raman spectra have so far indicated highly heterogeneous molecular distributions in a *S. pombe* cell. Such molecular distributions are more clearly and accurately displayed by Raman mapping patterns. In the Raman mapping experiment, the focused laser spot scans the area including the whole cell. The Raman intensities collected at each point are combined to construct two-dimensional maps of the Raman intensity distributions that directly reflect the molecular distributions. Figure 10 shows the Raman mapping results of a *S. pombe* cell in the G1/S phase. The mapping patterns of six Raman bands are presented: 1602 (Figure 10c), 1446 (Figure 10d), 1301 (Figure 10e), 1003 (Figure 10f), 891 (Figure 10g), and 426 cm^{-1} (Figure 10h). The Raman intensities are indicated by rainbow colors with red showing the highest intensity and blue the lowest. The optical microscope image (Figure 10a) and the GFP fluorescence image (Figure 10b) of mitochondria are also included as references. A *S. pombe* cell with GFP-labeled mitochondria was used in this mapping experiment.

The GFP image in Figure 10b shows that mitochondria exist densely in the central part being separated by the

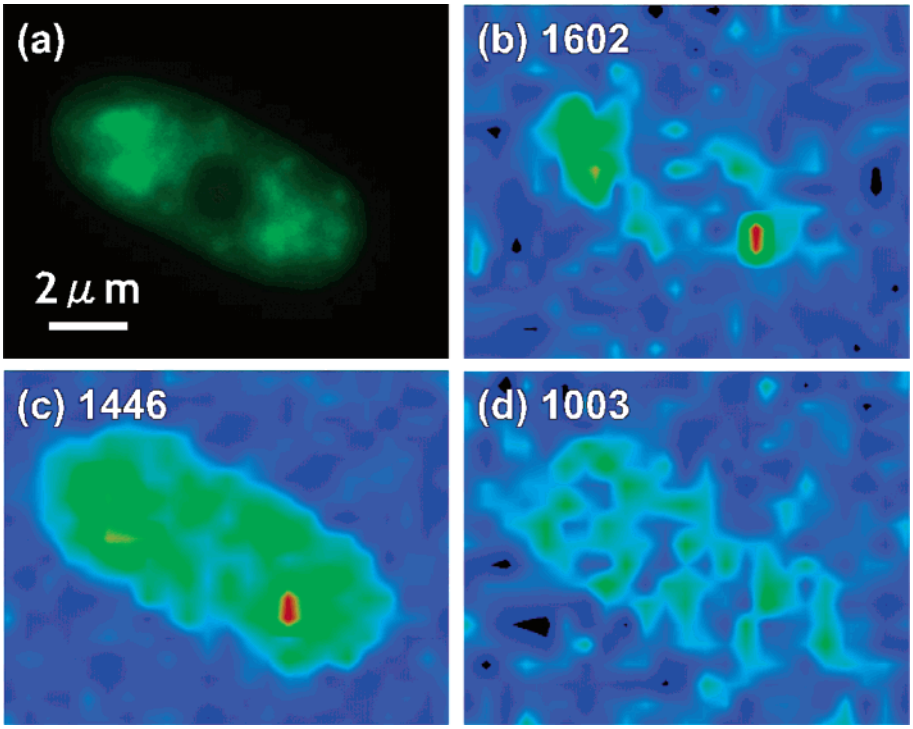

FIGURE 11: Raman mapping of a living G2 phase *S. pombe* cell: (a) GFP image, (b) 1602 cm^{-1}, (c) 1446 cm^{-1}, and (d) 1003 cm^{-1}.

septum. They also exist in smaller amounts at the two ends of this cell. The mapping pattern in Figure 10c shows that the 1602 cm^{-1} band is strong only in the brightest regions in the GFP image in Figure 10b, indicating that the species responsible for the 1602 cm^{-1} band is localized in the mitochondria. The images of the phospholipid bands at 1446 (Figure 10d) and 1301 cm^{-1} (Figure 10e) consist of two different patterns. One is the red (high-intensity) pattern similar to that in Figure 10b and reflects the distribution of mitochondria. The other is the green (medium-intensity) pattern that makes the shape of the cell. The red pattern is consistent with the extremely high concentration of phospholipids in mitochondria which have the structure composed of outer and inner membranes. The green pattern is ascribed to the other organelles and cytoplasm which span the whole cell. They contain phospholipids, but at lower concentration, than mitochondria, resulting in a medium-intensity distribution of the 1446 and 1301 cm^{-1} bands. There must also be contributions from the CH bending intensities of proteins and other molecules to the green patterns in panels d and e of Figure 10. The mapping pattern in Figure 10f of the 1003 cm^{-1} band is solely due to proteins and is not contaminated by the bands of other molecules. It seems that proteins are distributed almost evenly in the cell. The Raman mapping patterns of the 891 cm^{-1} band (Figure 10g) and the 426 cm^{-1} band (Figure 10h) produce the image of the septum. Although both of the 891 and 426 cm^{-1} bands are observed in the spectrum in Figure 7b, they seem to arise from different molecular species. The species that gives rise to the band at 891 cm^{-1} exists both in the septum and in the cell wall. The 426 cm^{-1} band, on the other hand, seems to arise from a species that exists only in the septum. These pieces of information on the molecular compositions will be a clue in understanding the structure and formation processes of a septum.

All the Raman mapping patterns in Figure 10 are indicative of molecular distributions symmetric with respect to the center of the *S. pombe* cell. Such symmetry has also been found for the other cell cycle stages. Figure 11 shows the mapping results for a G2 phase cell with its mitochondria labeled with GFP. The Raman mapping patterns for the 1602 cm^{-1} band (Figure 11b), the phospholipid band at 1446 cm^{-1} (Figure 11c), and the protein band at 1003 cm^{-1} (Figure 11d) are displayed as well as the fluorescence image (Figure 11a) of the cell. The three Raman mapping patterns are all symmetric with respect to the center, where the nucleus is located. This mapping experiment confirms the discussion in the preceding section; the *S. pombe* cell is prepared for the future division well beforehand, as early as in the G2 phase, so that the synthesized molecules and organelles are evenly distributed to the two moieties of the cell when the division starts. It is of great interest how each part of a cell communicates with each other to evolve synchronously to maintain the symmetry of the whole cell.

It must also be noted that the pattern of the 1602 cm^{-1} band (Figure 11b) does not entirely coincide with the GFP image (Figure 11a) and the Raman mapping pattern of the phospholipid band (Figure 11c). There are two large spots in the GFP image (Figure 11a), similar in size and brightness, in the left part of the cell, indicating that two groups of mitochondria exist at similar concentrations. The same is true for the map obtained with the 1446 cm^{-1} band (Figure 11c). On the other hand, the 1602 cm^{-1} band is strong only in the lower group of mitochondria. The Raman mapping by the 1602 cm^{-1} band does not merely show the mitochondrial distribution in a cell but points selectively to the metabolically active mitochondria. In other words, we are able to visualize the metabolic activity of mitochondria by mapping the intensity of the 1602 cm^{-1} band.

Thus, the Raman mapping technique provides us with detailed information about the spatial distribution of different

molecular species, simultaneously, in a living cell. It does not need any dyeing or labeling and hence can measure the cell really in vivo. Moreover, it can even visualize the mitochondrial metabolic activity in a cell by using the 1602 cm^{-1} band. The only drawback of the Raman mapping technique is the lack of fast time resolution. At this stage, it takes as long as 20 min to scan the whole cell, and therefore, it is only applicable to a cell whose cell cycle is deliberately stopped. We are now aiming to develop a faster technique based on direct Raman imaging and/or nonlinear Raman scattering.

CONCLUSIONS

The molecular compositional and structural information about organelles in fission yeast, *S. pombe*, has been obtained by observing the time- and space-resolved Raman spectra directly from single living cells by using a confocal Raman microspectrometer. The space-resolved Raman spectra of cells in different cell cycle phases show that fission yeast nuclei are dominated by proteins and their structures differ depending upon the cell cycle stage. They also show that the bilayer membrane of fission yeast mitochondria has a structure analogous to the structure of those in the liquid crystal state and/or in the liquid state. Such detailed molecular-level information can never be obtained with any other existing methods. Both the dividing and the dying process of *S. pombe* have been studied by the time- and space-resolved Raman measurements. The changes in molecular composition in the central part of a cell have been successfully traced, showing the transformation of the central part of the cell from a dividing nucleus to cytoplasm and mitochondria and finally to a septum. The maturing process of the septum has also been monitored. The addition of a respiration inhibitor, KCN, affects a mitochondrion of a living yeast cell in two steps: the disappearance of the 1602 cm^{-1} band showing the effect of respiration inhibition followed by the changes in the phospholipids bands indicating the destruction of the mitochondrial bilayer membrane. Although the origin of the 1602 cm^{-1} band is not yet clear, it might well be called the *Raman spectroscopic signature of life* (*5*). It is likely that this band was not reported before because the cell samples used in the previous studies were not actually living or were not under proper physiological conditions. Finally, it has been demonstrated that the Raman mapping method can visualize not only the distribution of molecules existing in a cell but also the more metabolically active regions of mitochondria. It does not require any dyeing or genetic manipulation of the cell and therefore looks into a living cell really in vivo.

ACKNOWLEDGMENT

We thank Professor Takashi Ogura for providing us with the sample of cytochrome *a*.

REFERENCES

1. von Lindner, P. (1893) *Schizosaccharomyces pombe* n. sp., ein neuer gährungserreger, *Wochenschr. Brau. 10*, 1298−1300.
2. Kriegmaier, M., Zimmermann, M., Wolf, K., Zimmermann, U., and Sukhorukov, V. L. (2001) Dielectric spectroscopy of *Schizosaacharomyces pombe* using electrorotation and electroorientation, *Biochim. Biophys. Acta 1568*, 135−146.
3. Huang, Y.-S., Karashima, T., Yamamoto, M., and Hamaguchi, H. (2003) Molecular-level pursuit of yeast mitosis by time- and space-resolved Raman spectroscopy, *J. Raman Spectrosc. 34*, 1−3.
4. Xie, C., and Li, Y.-q. (2003) Confocal micro-Raman spectroscopy of single biological cells using optical trapping and shifted excitation difference techniques, *J. Appl. Phys. 94*, 6138−6142.
5. Huang, Y.-S., Karashima, T., Yamamoto, M., Ogura, T., and Hamaguchi, H. (2004) Raman spectroscopic signature of life in a living yeast cell, *J. Raman Spectrosc. 35*, 525−526.
6. Maquelin, K., Choo-Smith, L.-P., van Vreeswijk, T., Endtz, H. P., Smith, B., Bennett, R., Bruining, H. A., and Puppels, G. J. (2000) Raman spectroscopic method for identification of clinically relevant microorganisms growing on solid culture medium, *Anal. Chem. 72*, 12−19.
7. Schuster, K. C., Urlaub, E., and Gapes, J. R. (2000) Single-cell analysis of bacteria by Raman microscopy: Spectral information on the chemical composition of cells and on the heterogeneity in a culture, *J. Microbiol. Methods 42*, 29−38.
8. Lutz, M. (1977) Antenna chlorophyll in photosynthetic membranes: A study by resonance Raman spectroscopy, *Biochim. Biophys. Acta 460*, 408−430.
9. Puppels, G. J., de Mul, F. F. M., Otto, C., Greve, J., Robert-Nicoud, M., Arndt-Jovin, D. J., and Jovin, T. M. (1990) Studying single living cells and chromosomes by confocal Raman microspectroscopy, *Nature 347*, 301−303.
10. Mohacek-Gresev, V., Bozac, R., and Puppels, G. J. (2001) Vibrational spectroscopic characterization of wild growing mushrooms and toadstools, *Spectrochim. Acta 57A*, 2815−2829.
11. Cheng, J.-X., Jia, Y. K., Zheng, G., and Xie, X. S. (2002) Laser-scanning coherent anti-stokes Raman scattering microscopy and applications to cell biology, *Biophys. J. 83*, 502−509.
12. Puppels, G. J., Olminkhof, J. H. F., Segers-Nolten, G. M. J., Otto, C., de Mul, F. F. M., and Greve, J. (1991) Laser irradiation and Raman spectroscopy of single living cells and chromosomes: Sample degradation occurs with 514.5 nm but not 660 nm laser light, *Exp. Cell Res. 195*, 361−367.
13. Feofanov, A. V., Grichine, A. I., Shitova, L. A., Karmakova, T. A., Yakubovskaya, R. I., Egret-Charlier, M., and Vigny, P. (2000) Confocal Raman microspectroscopy and imaging study of theraphthal in living cancer cells, *Biophys. J. 78*, 499−512.
14. Erckens, R. J., Jongsma, F. H. M., Wicksted, J. P., Hendrikse, F., March, W. F., and Motamedi, M. (2001) Raman spectroscopy in ophthalmology: From experimental tool to applications *in vivo*, *Laser Med. Sci. 16*, 236−252.
15. Notingher, I., Verrier, S., Romanska, H., Bishop, A. E., Polak, J. M., and Hench, L. L. (2002) *In situ* characterisation of living cells by Raman spectroscopy, *Spectroscopy 16*, 43−51.
16. Arikan, S., Sands, H. S., Rodway, R. G., and Batchelder, D. N. (2002) Raman spectroscopy and imaging of β-carotene in live corpus luteum cells, *Anim. Reprod. Sci. 71*, 249−266.
17. Shafer-Peltier, K. E., Haka, A. S., Fitzmaurice, M., Crowe, J., Myles, J., Dasari, R. R., and Feld, M. S. (2002) Raman microspectroscopic model of human breast tissue: Implications for breast cancer diagnosis *in vivo*, *J. Raman Spectrosc. 33*, 552−563.
18. Verrier, S., Notingher, I., Polak, J. M., and Hench, L. L. (2004) *In situ* monitoring of cell death using Raman microspectroscopy, *Biopolymers 74*, 157−162.
19. Yaffe, M. P., Stuurman, N., and Vale, R. D. (2003) Mitochondrial positioning in fission yeast is driven by association with dynamic microtubules and mitotic spindle poles, *Proc. Natl. Acad. Sci. U.S.A. 100*, 11424−11428.
20. Deng, H., Bloomfield, V. A., Benevides, J. M., and Thomas, G. J., Jr. (1999) Dependence of the Raman signature of genomic *B*-DNA on nucleotide base sequence, *Biopolymers 50*, 656−666.
21. Duffus, J. H. (1975) The isolation of yeast nuclei and methods to study their properties, in *Methods in Cell Biology* (Prescott, D. M., Ed.) Vol. 12, pp 77−97, Academic Press, New York.
22. Carey, P. R. (1982) Raman studies of proteins, in *Biochemical applications of Raman and resonance Raman spectroscopies*, pp 76−96, Academic Press, New York.
23. Larsson, K., and Rand, R. P. (1973) Detection of changes in the environment of hydrocarbon chains by Raman spectroscopy and its application to lipid−protein systems, *Biochim. Biophys. Acta 326*, 245−255.
24. Maiti, N. C., Apetri, M. M., Zagorski, M. G., Carey, P. R., and Anderson, V. E. (2004) Raman spectroscopic characterization of secondary structure in natively unfolded proteins: α-Synuclein, *J. Am. Chem. Soc. 126*, 2399−2408.

25. Dunker, A. K., and Obradovic, Z. (2001) The protein trinity: linking, function and disorder, *Nat. Biotechnol. 19*, 805−806.
26. Jeong, H., Mason, S. P., Barabási, A.-L., and Oltvai. Z. N. (2001) Lethality and centrality in protein networks, *Nature 411*, 41.
27. Lippert, J. L., and Peticolas, W. L. (1971) Laser Raman investigation of the effect of cholesterol on conformational changes in dipalmitoyl lecithin multilayers, *Proc. Natl. Acad. Sci. U.S.A. 68*, 1572−1576.
28. Siamwiza, M. N., Lord, R. C., Chen, M. C., Takamatsu, T., Harada, I., Matsuura, H., and Shimanouchi, T. (1975) Interpretation of the doublet at 850 and 830 cm^{-1} in the Raman spectra of tyrosyl residues in proteins and certain model compounds, *Biochemistry 14*, 4870−4876.
29. Gaber, B. P., and Peticolas, W. L. (1977) On the quantitative interpretation of biomembrane structure by Raman spectroscopy, *Biochim. Biophys. Acta 465*, 260−274.
30. Takai, Y., Masuko, T., and Takeuchi, H. (1997) Lipid structure of cytotoxic granules in living human killer T lymphocytes studied by Raman microspectroscopy, *Biochim. Biophys. Acta 1335*, 199−208.
31. Tasumi, M., Shimanouchi, T., and Miyazawa, T. (1962) Normal vibrations and force constants of polymethylene chain, *J. Mol. Spectrosc. 9*, 261−287.
32. Snyder, R. G., and Schachtschneider, J. H. (1963) Vibrational analysis of the *n*-paraffins. I. Assignments of infrared bands in the spectra of C_3H_8 through *n*-$C_{19}H_{40}$, *Spectrochim. Acta 19*, 85−116.
33. Snyder, R. G. (1967) Vibrational study of the chain conformation of the liquid *n*-paraffins and molten polyethylene, *J. Chem. Phys. 47*, 1316−1360.
34. Cherney, D. P., Conboy, J. C., and Harris, J. M. (2003) Optical-trapping Raman microscopy detection of single unilamellar lipid vesicles, *Anal. Chem. 75*, 6621−6628.
35. Northcote, D. H., and Horne, R. W. (1952) The chemical composition and structure of the yeast cell wall, *Biochem. J. 51*, 232−236.
36. Dauchez, M., Derreumaux, P., Lagant, P., Vergoten, G., Sekkal, M., and Legrand, P. (1994) Force-field and vibrational spectra of oligosaccharides with different glycosidic linkages. Part I. Trehalose dihydrate, sophorose monohydrate and laminaribiose, *Spectrochim. Acta 50A*, 87−104.
37. Dauchez, M., Lagant, P., Derreumaux, P., Vergoten, G., Sekkal, M., and Sombret, B. (1994) Force-field and vibrational spectra of oligosaccharides with different glycosidic linkages. Part II. Maltose monohydrate, cellobiose and gentiobiose, *Spectrochim. Acta 50A*, 105−118.
38. Campbell, M. K. (1999) Respiratory inhibitors block the flow of electrons in electron transport, in *Biochemistry*, 3rd ed., pp 561−564, Harcourt Brace & Co., Kent, U.K.
39. Carey, P. R. (1982) Raman, resonance Raman, and infrared spectroscopies, in *Biochemical applications of Raman and resonance Raman spectroscopies*, pp 6−8, Academic Press, New York.

BI050179W